PalArch's Journal of Archaeology of Egypt / Egyptology

# MULTI-CLASS BRAIN CANCER CLASSIFICATION USING DEEP LEARNING CONVOLUTIONAL NEURAL NETWORK

*V.K. Deepak*[1*], *R. Sarath*[2]

[1*]Research Scholar, Department of Electronics & Communication, Noorul Islam Centre for Higher Education, Thuckalay, Kumaracoil, Tamilnadu.

[2]Assistant Professor, Department of Electronics &Instrumentation, Noorul Islam Centre for Higher Education, Thuckalay, Kumaracoil, Tamilnadu.

[1*]deepakvk2@gmail.com,[2]sarathraveendran@gmail.com

**V.K. Deepak, R. Sarath. Multi-class Brain Cancer Classification Using Deep Learning Convolutional Neural Network-- Palarch's Journal of Archaeology of Egypt/Egyptology 17(7), 5341-5360. ISSN 1567-214x**

**Keywords: Hybrid Deformable Model with Fuzzy Method and Superpixel based Adaptive Fuzzy Clustering, Convolutional Neural Network, Tetrolet Transform, Harish Hawks Optimization.**

## ABSTRACT

Deep Learning is a modern area in machine learning that has been gaining more attention in the last few years. It has been commonly used in a variety of applications and has proved to be a strong machine learning method for numerousdifficulttroubles. In the context of screening services for prevention, Brain cancer tends to be one of women's leading causes of mortality and an amount of cash has been spent. Computer-assisted detection strategies adapted to date to improve diagnosis have not led to a significant improvement in performance metrics without multiple systematic readings. The use of advanced image processing techniques resulting from deep learning in this context represents a promising way to help diagnose brain cancer. The classifier was combined with the fuzzy system hybrid deformable model and superpixel-based adaptive clustering and the efficient feature extraction tool and Harish Hawks Optimization (HHO) Tetrolet Transform (TT) and the performance evaluation was very good overall performance steps. Experimental findings on MRI images indicate that the ResNet CNN model achieved a high degree of perfect processing.

## INTRODUCTION

Cancer can be described as accelerated, abnormal cell growth division inside the body. The development, as a mass, of these improper cell growth and brain tissue partitions is called a brain tumour. Although brain tumours are not very common, they are by far the most deadly cancers. Brain structure can be

scanned with Magnetic Resonance Imaging (MRI) scans or computed tomography (CT) scansThe MRI Clinical examination is more convenient than the CT clinical exam. The human body is not threatened by it since it does not use radiation. It is dependent on a magnetic field and a radio wave[1]. Brain tumours, on the other hand, are one of the major causes of mortality in humans. Evidence shows that if the cancerous tumor is accurately diagnosed and treated early, the likelihood of survival may be increased. In certain cases, the doctor will provide stroke care instead of tumour care. Detection of the tumour is therefore necessary for care. The average life span of the person affected by the brain tumour will increase if it is identified early[2]. Therefore, an effective medical image segmentation technique with certain preferred characteristics is needed, such as minimal human involvement, fast computer processing, precise and efficient partition performance. Research teams have actually suggested numerous technological approaches to the detection and classification of brain tumours using brain MRI images, as medical images could be scanned and uploaded to the device. In the last few centuries, however, support Vector Machine (SVM) and Neural Networks (NN) are commonly used approaches to their effective success [3]. But currently, as deep learning model can be powerful, deep learning (DL) models have created an interesting trend in artificial intelligence. Convolutionary neural networks (CNNs) are the most common class of image analysis models to date.

## RELATED WORK

The medical image analysis community has taken notice of these pivotal developments. Veeramuthuet al.[4] suggested the classification of brain images using the machine learning method and the study of brain structures. The method of Multi Level Discrete Wavelet Transform helps to decompose the image, and then extract the features. Using PNN-RBF training and classification process, the brain image is categorised whether the disease is of mild, benign or malignant stages. Sanjeev et al.[5] developed a hybrid approach. This hybrid approach involves discrete wavelet transformation (DWT) to be used to remove features, genetic algorithm to decrease the number of features and support vector machine (SVM) for classification of brain tumours. Gopal et al.[6] proposed approach based on feed forward back-propagation of the neural network (FFBPNN) to improve the efficiency of classification of motor imagery. In this field several methods of grouping for medical images are available such as artificial neural network (ANN), fuzzy c-means (FCM), support vector machine (SVM), decision tree, K-Nearest Neighbour (KNN) and Bayesian classification. Among, this ANN, SVM, and KNN are the supervised learning procedures. Another class is unsupervised learning for data clustering such as Self Organizing Map, K-means clustering. However, the transition from systems that use handmade features to systems that learn data features has been gradual. Before AlexNet's breakthrough, several different techniques for learning features were common. Bengio et al. [7] shall provide for a comprehensive analysis of these techniques. These include main component analysis, image patch clustering, dictionary approaches, and many more. Moosaet al.[8] will implement CNNs that are trained on an end-to - end basis only at the end of their analysis in a segment entitled Global Training of Deep Models. In this survey, we concentrate in particular on such deep-rooted models and do not include the more

conventional feature-learning methods applied to medical images. For a more general overview of the application of deep learning in health informatics, refer to Ravi et al. (2017)[9], where the analysis of medical imagery is briefly discussed, a dedicated examination of the application of deep learning to the analysis of medical imagery was reported by Shen et al. (2017)[10]. While they cover a significant amount of work, we feel that important areas of the field have not been mentioned.

***Problem Statement***

There are several obstacles to image segmentation and classification, such as creating a standardizedmodel that can be extended to all forms of images and purpose. Then again the deciding on the right technique for a particular type of image is a difficult problem. Therefore, for identification and classification of images, there is really no broadly agreed procedure. In the field of computer vision systems, it remains a major obstacle. The approach failed to consider classifying images of various pathological disorder, type and status of the disease. The system includes a lot of pure nodes that can result in overfitting. Designers suggested a deep learning principle to accomplish an automated brain tumour identification using brain MRI images and to evaluate its efficiency in order to overcome these problems.

***The Contribution of Proposed Work***

- By using a novel boosted adaptive anisotrophic diffusion filter, histogram equalizationthe image get enhanced.
- Segmentation is done in two phases. The first phase is brainsection; the tumour area is extracted using a hybrid deformable model with a fuzzy approach and a superpixel-based adaptive clustering.
- The features are extracted based on texture and tetrolet transform, and the extracted features are combined by using Harish hawks optimization algorithm.
- The suggested technique is intended to distinguish between normal brain tumours and abnormal brain MRI images by the CNN classifier.

Our proposed methodology is fully automatic and durable. No prior knowledge of the image is required on its features, quality, form and model. The proposed method is a very reliable brain tumour diagnostic system. The paper is structured as follows: the relevant work is shown in Section 2. Details of the proposed technique are defined in Section 3 and the performance metrics are described in Section 4. Section 5 includes descriptions of the experimentation and effects. The conclusion and future work are discussed in section 6.

## PROPOSED METHOD

The proposed system segments and classifies the brain tumor in multiple stages. First stage is Pre-processing here the noise present in the image is removed segmentation where the brain portion is extracted separately from the skull part and all other portion present in an image. After this, features are extracted and among those features, feature selection process involves. Finally classification method classifies the tumorous region is shown in figure 1.

***Pre-processing***

This phase is obtained by applying a set of basic processing techniques to the image prior to every advanced modeling purpose. It enhances the reliability of the image and reduces noise. Since brain scans are more delicate than other medical data, they should be of reduced distortion and of the largest quality [10]. This level, therefore, comprises of the two sub-stages:

- ***De-noising:***The MRI images are regularly obscured by disruptions such as Gaussian and Poisson noise[11]. Additive white Gaussian noise is presumed by the great majority of denoise approach. There are a few methods designed to remove Gaussian noise. The adaptive anisotrophic diffusion filter used here has been used. It is a non-linear filter that is used as an efficient way to eliminate noise. After the denoising process, the image is improved by a histogram equalisation technique [12].

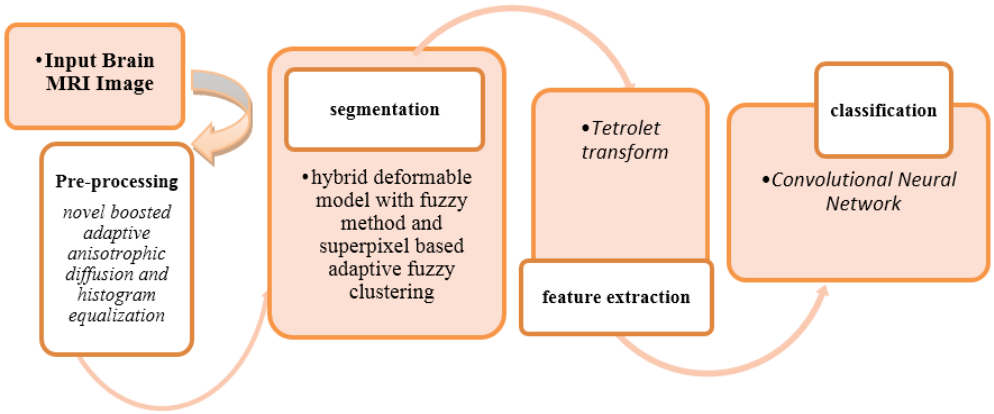


**Figure1** Overall Flow of Proposed Work

***Image Segmentation***

It is a highly complex process of distinguishing the various healthy brain tissues [24, 25], such as grey matter (GM), white matter (WM) and cerebrospinal fluid (CSF) from the tumour tissues in the brain MR images. In this job, a hybrid deformable model with a fuzzy approach and a super pixel-based adaptive cluster used to divide the image into five categories as it had great result.

- ***Hybrid Deformable Model with Fuzzy Method***

Deformable models have achieved considerable success in the fields of computer vision and pattern recognition. Deformable models can usually be split into two categories: explicit models and implicit models. The above deformable models were proposed primarily for the purpose of the reconstruction of shapes from volumetric data and for the segmentation of medical imagery. Current works primarily focus on static methods for shape reconstruction from point clouds [13]. They are either clear approaches using Delaunay Triangulation. Deformable models are dynamic models whose 2D or 3D forms develop under the influence of external forces and internal forces. Internal forces are measured within the form to keep it smooth. External forces

are calculated from the images to transfer the curve or the surface to the desired location.

The Fuzzy algorithm is still the most effective approach used in edge detection because it has a robust instability mechanism and retains far more information than the soft segmentation. The fuzzy c means algorithm was first created by Dunn and expanded to Bezdek. The test pixel in this methodology can be a part of two or more clusters with a different access coefficient. This algorithm is continuous in nature, produces a fuzzy fraction matrix, and requires an optimal solution cluster center[14]. y each iterative process, the cluster centre value and optimal solution are altered and halted when the distance between different consecutive object function values is below the predefined threshold value T. FCM method computes the optimum solution C partition by mitigating the error function fitness function within the group sum[12] and is categorized in below.

$$J_{FCM} = \sum_{k=1}^{n} \sum_{i=1}^{c} (v_{ik})^q \, d^2(X_k, V_i) \qquad (1)$$

where, $x = x_1, x_2, .., x_n \leq R$ represents dataset, n-number of data items, c-number of clusters; $2 \leq c < n, v_{i,k}$degree of membership of $X_k in \, i^{th}$ cluster, q-weighting exponent of each fuzzy member, and $v_i$prototype of center cluster i.

- ***Super Pixel based Adaptive Clustering***

The image is split into small equal blocks in the current technique. The Central Tendency Value (CTV) generally indicates the ability of the details to organise the system around with a key value. In the developed system, the CTV of each block is calculated using mean and median is used as the super pixel value of the corresponding block.

The CTV computed using mean $M_i$ represents the mean value of the i$^{th}$ block $B_i$ and given in Eqn. 2.

$$M_i = \frac{1}{n} \sum_{j=1}^{n} p_j^i \qquad (2)$$

Where, $i = 1; 2::m$ number of blocks of the image I. $p_j^i$ is the j pixel value of the ith block $B_i$ in the given image I. Where $j = 1; 2 \ldots n$, number of pixels in the ith block of the image I. The CTV computed using median $med_i$represents the median value of i$^{th}$ block bi and calculated using the following steps.

1. Sort the pixel values of i$^{th}$ block $B_i$ of the given image I.
2. After sorting the pixel values in the block $B_i$, the CTV calculated using the median $med_i$ is given in the Eqn. 36

$$med_i = \begin{Bmatrix} \frac{1}{2}\left(p_i^{\frac{n}{2}} + p_i^{\frac{n}{2}+1}\right) & if \; n \, mod 2 == 0 \\ p_i^{\frac{n}{2}} & if \; n \, mod 2 \neq 0 \end{Bmatrix} \qquad (3)$$

Where, n = 1; 2: number of pixels of i[th] block$B_i$. $p_i^{\frac{n}{2}} is (n/2)^{th}$pixel value of i[th] block $B_i . p_i^{\frac{n}{2}+1} is \left(\frac{n}{2}+1\right)^{th}$ Pixel value of i[th] blocks $B_i . p_i^{\frac{n+1}{2}} is \left(\frac{n+1}{2}\right)^{th}$ Pixel value of i[th] blocks $B_i$ and i = 1; 2...m, number of blocks of the image

The CTV calculated utilizing mode $med_i$ describes the norm quality of the i[th] section of image I and is measured as one of the most common image pixel $p_i$ in the ith section $B_i$ of image I. In which $i = 1; 2 \ldots n$and m are a range of modules in the image. The correct data is now shown using super pixels of blocks measured using CTV. Through spectral clustering, these super pixels are divided. Knowledge on the segmentation of the super pixels are identified in the following subdivision. Adaptive clustering is introduced to the super pixel values of the blocks of the image. In order to acquire segmented tumours region superpixel detection is carried out. The proposed approach, a clustering algorithm, overcomes all the weaknesses of the existing algorithm. It often produces the same segmentation outcome that is independent of every particular membership values. The segmentation accuracy is improved, as the impact of the strength of the image is reduced. Finally, easy, quick and typical are morphological operations used. The proposed segmentation method much less computation complexity.

***Feature Extraction***

After segmentationthe dividedtumour are extracted using texture [17] and Tetrolet Transform (TT) [16] features. TT has the advantage of extracting the most important features in various directions and scales as it provides localised signal frequency information using cascaded high-pass and low-pass filter banks to extract features in a hierarchical manner[13].

- ***Texture Features***

It is a statistical method for analysing images in which the algorithm relates two pixels to an image by observing their occurrence in a given spatial area. Using these relations, a co-occurrence matrix (CCM) is generated and then statistical measurements are derived from it. CCM is the matrix in which each point represents the frequency of the number of times the pixel is observed at that point. GLCM uses this approach to evaluate its functionality. There are several texture features available, but in this study only four features are used: energy, contrast, correlation and homogeneity[14].

$$\text{Energy} \sum_{i=0}^{G-1} \sum_{j=0}^{G-1} [\mathrm{p(i,j)}]^2 \qquad (4)$$

$$Homogenity = -\sum_{i=0}^{G-1} p(i) \log_2[\mathrm{p(i)}] \qquad (5)$$

$$\text{Correlation} = \sum_{i=0}^{G-1} \sum_{i=0}^{G-1} \frac{\mathrm{ij\ p(i,j)} - \mu_x \mu_y}{\sigma_x \sigma_y} \qquad (6)$$

$$\text{Contrast} = \sum_{i=0}^{G-1} \sum_{j=0}^{G-1} (\mathrm{i-j})\mathrm{p(i,j)} \qquad (7)$$

Mean, standard deviation, skewness, kurtosis, and entropy are referred to as colour attributes. Entropy gives the amount of image information that is needed for the compression of the image. These characteristics are derived by

a colour moment (CM) descriptor. The statistical characteristics (FOS) of the equations are given below:

$$\text{Mean}\mu = \sum_{i=0}^{G-1} \text{i p(i)}) \quad (8)$$

$$\text{Variance } \sigma^2 = \sum_{i=0}^{G-1} (\text{i} - \mu)^2 \text{p(i)} \quad (9)$$

$$\text{Skewness } \mu_3 = \sigma^{-3} \sum_{i=0}^{G-1} (\text{i} - \mu)^3 \text{p(i)} \quad (10)$$

$$\text{Kurtosis}\mu_4 = \sigma^{-4} \sum_{i=0}^{G-1} (\text{i} - \mu)^4 \text{p(i)} \quad (11)$$

$$\text{Entropy} = \text{H} = -\sum_{i=0}^{G-1} \sum_{j=0}^{G-1} \text{p (i, j)} \log_2[p(i)] \quad (12)$$

- ***Tetrolet Transform (TT)***

Following steps, the multi-scale tetrolet decomposition of the specified input noisy image is obtained $\text{g} = [\text{g(x, y)}]_{x,y=1}^{N}$ with$N = 2^k$, K$\in N$, while the tetromino covering c and the amount of decomposition rates J is obtained. We're starting with the image input $\text{g} = [\text{g(x, y)}]_{x,y=1}^{N}$. We do the following calculations at the j-th level, j=1.....,,

1. Divide the low-pass image $g^{j-1}$ into 4 ×4 blocks, $\text{Q}_{\text{m,n}} m$, = 1…$\frac{N}{2^{j+1}}$
2. In each block$\text{Q}_{\text{m,n}}$ the low-pass part for tetromino covering is calculated by c

$$g^{j,(c)} = (g^{j,(c)}[v])^3{}_{v=0} with g^{j,(c)}[v] = \sum_{(x',y')\in I_v^{(c)}} \varphi_{I_v}^{(c)} [x', y'] g^{j-1}[x', y'] \quad (13)$$

as well as the three high-pass parts for l = 1, 2, 3

$$s^{j,(c)} = (s_l{}^{j,(c)}[v])^3{}_{v=0} with s_l{}^{j,(c)}[v] = \sum_{(x',y')\in I_v^{(c)}} \psi_{I_v}^{(c)} [x', y'] g^{j-1}[x', y'] \quad (14)$$

We save the covering c for each block$\text{Q}_{\text{m,n}}$, which is used for partitioning, since this information is required at reconstruction time.

3. To enable additional levels of the tetrolet decomposition algorithm to be applied, we rearrange the vector entries $g^{\text{j,(c)}}$ and $S_l^{\text{j,(c)}}$ into 2 × 2 matrices using a reshape function R,

$$g_{l/Q_{m,n}}^{j} = R g^{j,(c)} = \begin{pmatrix} g^{j,(c)}[0] & g^{j,(c)}[1] \\ g^{j,(c)}[2] & g^{j,(c)}[3] \end{pmatrix}. \quad (15)$$

and in the same way

$$S_{l/Q_{m,n}}^{j} = R\left(S_l^{j.(c)}\right), \text{l=1,2,3.} \quad (16)$$

4. After finding a tetrolet decomposition in every block$\text{Q}_{\text{m,n}} m$, = 1…$\frac{N}{2^{j+1}}$ we store the low-pass matrix

$g^j = \left(g_{l/_{Q_{m.n}}}^{j}\right)_{m,n=1}^{\frac{N}{2j+1}}$& the high-pass matrices $s^j = \left(s_{l/_{Q_{m.n}}}^{j}\right)_{m,n=1}^{\frac{N}{2j+1}}$l=1,2,3, replacing the low-pass image $g^{j-1}$by the matrix$\begin{pmatrix} g^j & s_2^j \\ s_1^j & s_3^j \end{pmatrix}$. In this way we obtained one low pass image (subband) **g***j* and three high=pass subbands$s_1^j, s_2^j and s_3^j$ in the decomposition level j.

5. After apply a shrinkage procedure to the tetrolet coefficients after a suitable number of decomposition steps.
6. Apply steps 1 to 4 to the low pass image up to the appropriate number of decomposition level and reconstruct the filter bank algorithms.

***Feature Selection***

The method used to pick a subset function from the database is generally known as the selection of features. Feature selection can be defined as an optimization problem that aims to reduce computation time and improve accuracy with a feature optimization algorithm by eliminating redundant, unrelated and noisy features.

- ***Harris Hawks Optimization***

Harris Hawks Optimization (HHO) is an innovative, gradient-free, population-based optimization methodology that mimics the hunting theme of Harris Hawks bird species. HHO was recently launched by Heidari et al. in 2019[14]. The system applies the Harris hawks' actions of prey in existence, such as prognostication, exploitation, and unexpected swoop down techniques. Like other metaheuristic algorithms, HHO has two distinct components: discovery and exploitation, as shown in Figure 2. However, HHO has two stages of discovery and four stages of extraction, which are described in detail as follows.

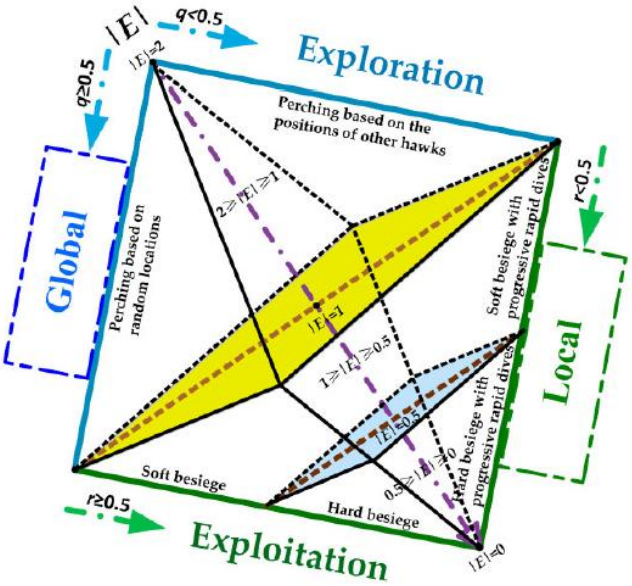


**Figure 2**Exploration and Exploitation Phases of Harris Hawks Optimization (HHO)

- ***Initialization Phase:***The optimization problem and its optimal solution are described in this step. In addition, the meanings for the variables are allocated and the population size is produced.
- ***Exploration Phase:***This is the phase by which Harris Hawks is searching for a target (a rabbit). The hawks have powerful eyes that can enable them identify and monitor the prey, but it's really hard to see the prey. In this case, the hawks are trying to monitor the spot, expecting to see the prey.

Basically, in each version, all Harris hawks are the nominee alternatives and the highest accuracy is calculated on the basis of the prey planned for each of them.

- ***Exploitation Phase:*** In this step, the Harris hawks strike the prey on the grounds of the position identified in the initiation section. But the rabbit is already trying to run, and the hawks are following a chase tactic. Thus, HHO is developed on the basis of four possible methods of fighting strategies. Independent quantities indicate which technique to apply, r and. Although the escape energy of the rabbit is, r refers to the escape rate, where r < 0:5 suggests a higher likelihood for the rabbit to exit safely and r ≤0:5 for inability to exit.

### *Classification*

Classification is the process of classifying the items according to its type and pattern. Selecting the suitable classifier improved performance results in accuracy for various datasets. Here, the tumors are classified as benign and malignant tumor. So the proposed system combines CNN classification technique to make the process more efficient than the existing process. CNN helps to increase the accuracy in detecting the exact tumor affected area.

- ***Proposed CNN Model for Multi-Class Brain Cancer Classification***

A Convolutional Neural Network (CNN) is a feed-forward neural setup makes by Kunihiko Fukushima in 1980 and modified by Yann LeCan et al. in 1998. CNN comprises of 6 forms of layers: an input layer, a convolutionary layer, a non-linear layer, a pooling layer, a fully linked layer, and a layer of output. The traditional Cnn model displays in figure 3. One of the most successful deep learning architectures in which successive sources of neurons are formed in a precise way is Convolutionary Neural Networks (CNNs). They have shown that they are able to demonstrate an excellent generalisation capability for massive data sets with millions of images[19]. These results originate primarily from the specific CNN architecture, which calculates the dynamic topology of tasks applicable to the area of computer vision that handle two-dimensional images. In terms of multi-channel colour images, other variables may also be assessed.

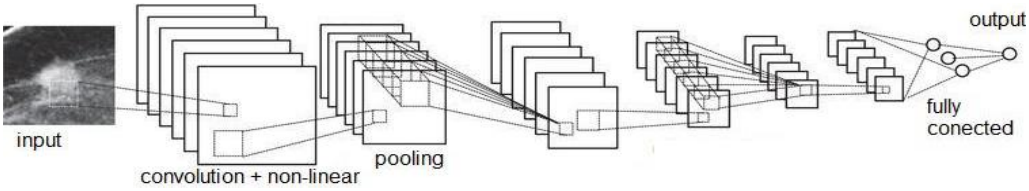


**Figure3**Convolutional Neural Network Architecture

To develop CNN, using the feed forward step, evaluate the linear model and maximize the objective functions using backward propagation methods, particularly the gradient of a reliable algorithm. [20-23].

By implementing Volterra's theory the feasibility of introducing an appropriate convolution system to improve the learning ability of CNNs, which was used to research non-linear physiological processes and adapt it to the spatial domain.

A second order Volterra sequence for our proposed Convolution provided a patch on the input$I \in IR^{k_h \times k_w}$ with n elements (n=$k_h . k_w$), reshaped as a vector $X \in IR^n$:

$$X = [x_1 x_2 \dots x_n]^T \qquad (17)$$

the input-output characteristics of a linear filter is:

$$y(x) = \sum_{i=1}^{n} \left(w_1^i x_i\right) + b \qquad (18)$$

Where $w_1^i$is the weights of functional forms of the convolution found in a vector$w_1$, and b is the bias. In our approach this concept is broadened in the following quadratic form:

$$y(x) = \sum_{i=1}^{n} \left(w_1^i x_i\right) + \sum_{i=1}^{n} \sum_{j=1}^{n} \left(w_2^{i,j} x_i x_j\right) + b \qquad (19)$$

Where, $w_2^{i,j}$ is the weight of 2nd-order elements in the filter. for a command r filter based on Volterra is:

$$n_v = \frac{(n+r)!}{n!r!} \qquad (20)$$

In a more compact form, (3) is written as:

$$\mathrm{y(x)} = \underbrace{X^T w_2 X}_{quadratic\ \ term} + \underbrace{W_1^T X}_{linear\ \ term} + b \qquad (21)$$

While for the Volterra kernels we have:

$$\mathbf{w}_2 = \begin{bmatrix} w_2^{1,1} & w_2^{1,2} & \cdots & w_2^{1,n} \\ 0 & w_2^{2,2} & \cdots & w_2^{2,n} \\ \vdots & \vdots & \ddots & \vdots \\ 0 & 0 & \cdots & w_2^{n,n} \end{bmatrix} \qquad (22)$$

Containing the coefficients $w_2^{\mathrm{i;j}}$ of the quadratic term, and:

$$w_1^T = [w_1^1 w_1^2 \dots . w_1^n] \qquad (23)$$

Containing the coefficients $w_1^i$ of the linear term. The proposed convolution's output can thus be rewritten as:

$$y(\mathbf{x}) = \begin{bmatrix} w_2^{1,1} \\ w_2^{1,2} \\ w_2^{1,3} \\ \vdots \\ w_2^{n,n} \end{bmatrix}^T \begin{bmatrix} x_1 x_1 \\ x_1 x_2 \\ x_1 x_3 \\ \vdots \\ x_n x_n \end{bmatrix} + \begin{bmatrix} w_1^1 \\ w_1^2 \\ w_1^3 \\ \vdots \\ w_1^n \end{bmatrix}^T \begin{bmatrix} x_1 \\ x_2 \\ x_3 \\ \vdots \\ x_n \end{bmatrix} + b \qquad (24)$$

Note that superscripts (i; j) to weights $w_2^{\mathrm{i;j}}$ denote correspondence to the spatial positions of the input elements $x_i$ and $x_j$ that interact.

The mathematical equations of back propagation are as follows:

$$\frac{\partial y}{\partial w_1^i} = x_i \frac{\partial y}{\partial w_2^{i,j}} = x_i x_j \qquad (25)$$

$$\frac{\partial y}{\partial x_i} = w_1^i + \sum_{k=1}^{i}(w_2^{k,i} x_k) + \sum_{k=1}^{n}(w_2^{i,k} x_k) \quad (26)$$

## PERFORMANCE MATRICS

Following equation shows the percentage of the actual lesion that has been truly detected by the automated method. The performance metrics result of the proposed method is shown in table 4. The performance measures of the proposed techniques are compared with the existing method the comparison is shown in table 5.

$$\text{Jaccard Index} = J(A,B) = \frac{S(A \cap B)}{S(A \cup B)} \quad (27)$$

$$\text{Dice Overlap Index (DOI)} = D(A,B) = 2X\frac{A \cap B}{A+B} \quad (28)$$

$$\text{Similarity Index} SI = \frac{2XTruepositive}{2Xtruepositive + falsepositive + falsenegative} \quad (29)$$

$$\text{Absolute Volume Measurement Error (AVME)} = \left(\frac{V_{automatic}}{V_{manual}} - 1\right) X\ 100\% \quad (30)$$

$$\text{Figure of Merit}(\varepsilon) = 1 - (\varepsilon) = 1 - \frac{|V_{manual} - V_{automatic}|}{V_{manual}} \quad (31)$$

$$Sensitivity = \frac{TP}{TP+FN} \times 100\% \quad (32)$$

$$Specificity = \frac{TN}{TN+FP} \times 100\% \quad (33)$$

$$Accuracy = \frac{TP+TN}{TP+FP+FN+TN} \times 100\% \quad (34)$$

$$Precision = \frac{TP}{TP+FP} \times 100\% \quad (35)$$

$$Recall = \frac{TP}{TP+FN} \times 100 \quad (36)$$

$$F - measure = \frac{2 * Precision * Recall}{Pr\ ecision + Recall} \quad (37)$$

where
TN is True Negative
TP is True positive
FP is False positive
FN is False negative

## EXPERIMENTAL RESULTS

- ***Data Sets***

Here three benchmark sets of data to monitor the efficiency of our segmentation technique. That the very first concerns the data gathering on Digital Imaging and Communications in Medicine (DICOM)]. DICOM consists of 22 images of neurological disorders. Both DICOM captured images are encoded with the JPEG2000 transfer format. Extension of DCM. There are no ground-based images of truth for the enclosed frames. The second data array is the Brain Web Data Set[35]. It contains digital brain MRI information focused on multiple anatomical models: normal and systemic sclerosis (MS). Full three- dimensional interests of the data were modeled using several components (T1-, T2-, and proton-density-(PD-)weighted) and a range of slice thicknesses, noise levels, and intensity non-uniformities.

- ***Simulation Outputs***

The following steps display the results obtained by giving the original brain MRI image from the database. Preprocessing techniques are applied to the sample images in order to reduce noise and boost the quality of the image (4 &

5). This step is followed by the segmentation of the tumour area from the images, Figure 6. The resulting features are extracted and reduced from the segmented images in Table 1. Finally, the classification technique is applied in order to achieve a higher degree of intensity and accuracy.

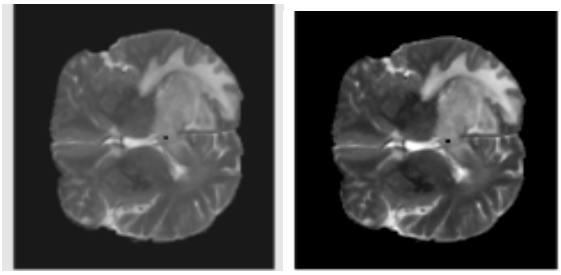

(a) (b)

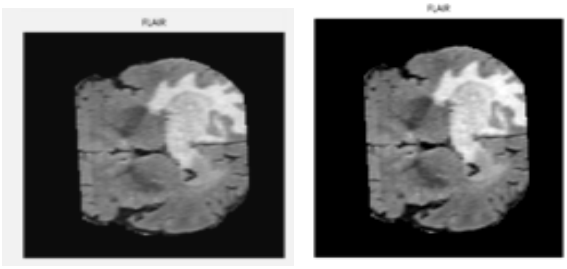

(a) (b)

**Figure4**Preprocessed Results of MRI Images

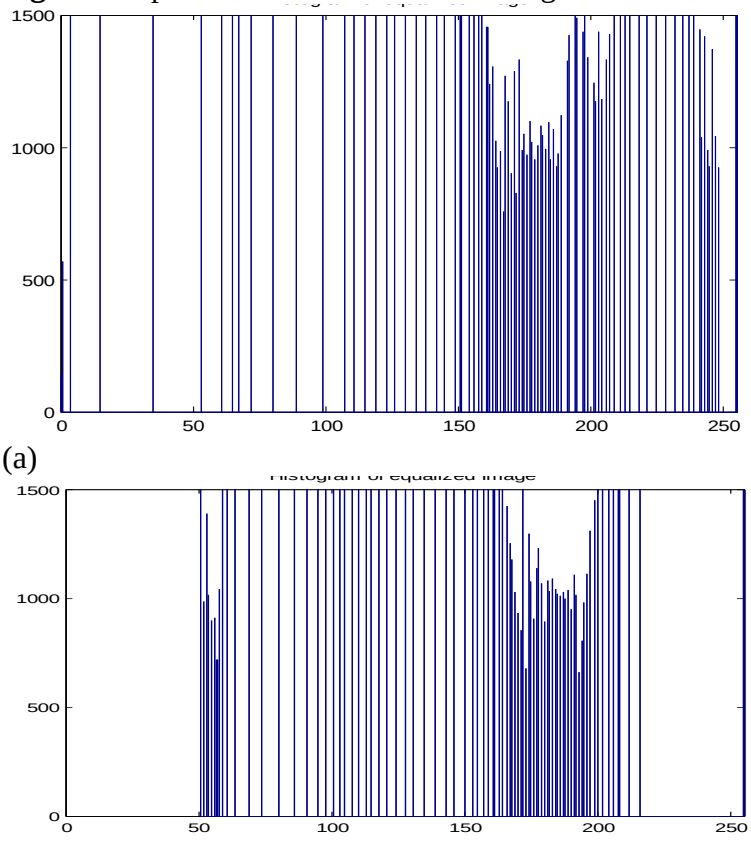


(a)

(b)

**Figure5**Histogram Plot Results of MRI Images

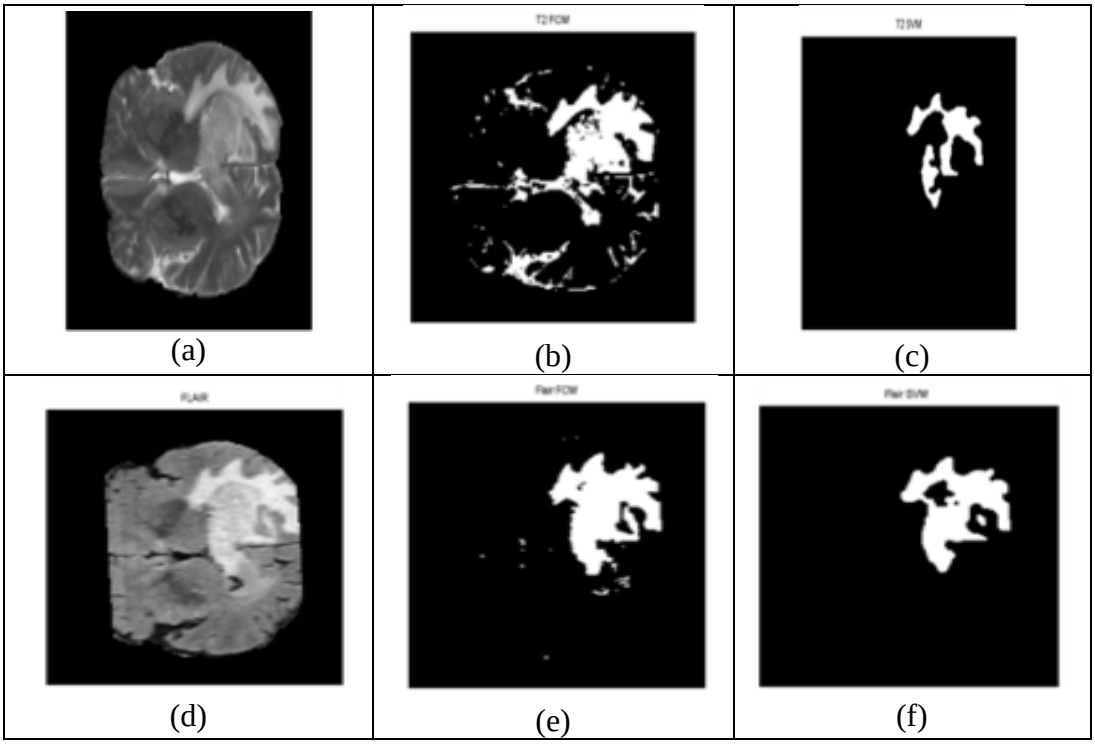


**Figure 6**(a) & (d) Input MRI Image, (b) & (e)Final Hybrid Deformable Model with Fuzzy Method, (c) & (f) Final Super Pixel based Adaptive Clustering Method Segmented Output

The evaluation matrices are Dice coefficient, jaccard index, absolute volume measurement error, figure of merit and spatial overlap to find out the segmentation efficiency. The volume measurement of segmented ROI'sand its ground truth values are shown intable 1&2. The obtained result of Dice coefficient is an average of 0.79and Jaccard index is 0.85. Both value shows betterment in the efficiency than hybrid deformable model with a fuzzy approach. The AVME is reduced and improved the figure of merit value with an average of 0.77. The spatial overlap shows an average of 0.91 and most of the evaluations show that superpixel-based adaptive clustering shows good result than hybrid deformable model with a fuzzy approach.

**Table 1** Obtained results of Evaluation matrices using hybrid deformable model with a fuzzy approach

| IMAGES | DICE COEFFICIENT | JACCARD INDEX | ABSOLUTE VOLUME MEASUREMENT ERROR | FIGURE OF MERIT | SPATIAL OVERLAP |
|---|---|---|---|---|---|
| 1 | 0.81 | 0.8 | 24.49 | 0.83 | 0.89 |
| 2 | 0.84 | 0.72 | -28.49 | 0.6 | 0.83 |
| 3 | 0.82 | 0.86 | -18.6 | 0.71 | 0.9 |
| 4 | 0.61 | 0.78 | -22.13 | 0.91 | 0.88 |
| 5 | 0.63 | 0.92 | -7.88 | 0.75 | 0.96 |
| 6 | 0.75 | 0.78 | 28.86 | 0.77 | 0.87 |
| 7 | 0.87 | 0.83 | 20.13 | 0.81 | 0.91 |
| 8 | 0.85 | 0.61 | -39.22 | 0.71 | 0.76 |

| | | | | | |
|---|---|---|---|---|---|
| 9 | 0.75 | 0.87 | -13.31 | 0.81 | 0.93 |
| 10 | 0.77 | 0.83 | -16.89 | 0.81 | 0.91 |

**Table 2**Result obtainedUsing Superpixel-based Adaptive Clustering in Terms various Evaluation Matrices

| **Images** | **Dice Coefficient** | **Jaccard Index** | **Absolute Volume Measurement Error (AVME)** | **Figure of merit (FoM)** | **Spatial overlap** |
|---|---|---|---|---|---|
| 1 | 0.84 | 0.87 | 14.25 | 0.83 | 0.93 |
| 2 | 0.79 | 0.87 | -13.01 | 0.6 | 0.93 |
| 3 | 0.91 | 0.84 | -14.92 | 0.71 | 0.91 |
| 4 | 0.88 | 0.76 | -23.63 | 0.91 | 0.87 |
| 5 | 0.52 | 0.98 | 1.55 | 0.75 | 0.99 |
| 6 | 0.84 | 0.81 | 22.99 | 0.77 | 0.9 |
| 7 | 0.8 | 0.76 | 32.21 | 0.81 | 0.86 |
| 8 | 0.71 | 0.77 | -22.79 | 0.71 | 0.87 |
| 9 | 0.9 | 0.96 | -4.44 | 0.81 | 0.98 |
| 10 | 0.78 | 0.83 | 20.81 | 0.81 | 0.91 |

From the table 4, it is inferred that the True Positive values of the image should always be higher for better results and the False Negative should be as low as possible. The experimental result proves that by using the Deep learning classifier, the overall accuracy is high related to traditional classifiers. From our experiments on different images, it is observed that the proposed method works well on both the cases when the objects in the image were indistinct and distinct from the background.

**Table 4** Comparison of Classifier values with Reference to the Confusion Matrix

| **Classifier** | **TP(%)** | **FP(%)** | **FN(%)** | **TN(%)** |
|---|---|---|---|---|
| **SVM** | 41.9 | 57.7 | 42.3 | 58.1 |
| **Back propagation** | 45.6 | 56.1 | 43.9 | 54.4 |
| **ANN** | 44.9 | 56.6 | 43.4 | 55.1 |
| **CNN** | 48.5 | 64.9 | 35.1 | 51.5 |

The efficiency and accuracy of the CNN classifier is shown in Figures 7 & 8. This CNN ResNet-50 template consists of five stages including one with a matrix multiplication block and an Identity block. Each convolution block has three layers of matrix multiplication, and each identity frame has three layers of convolution. The ResNet-50 has more than 23 million training parameters. The First Section of Resnet and the First Section of Convolution Layer Weights are shown in the figure. The average accuracy of CNN is 98.3 per cent. The proposed accuracy is in contrast with the state-of-the-art methods shown in Figure 9.

**Table 5**Feature Extraction Result

| **Ima** | **GLCM Feature** | **First Order Statistics(FOS) Feature** |
|---|---|---|

| ge No | | | | | | | | | |
|---|---|---|---|---|---|---|---|---|---|
| | **Contrast** | **Correlation** | **Energy** | **Homogeneity** | **Mean** | **Standard Deviation** | **Skewness** | **Kurtosis** | **Entropy** |
| **1** | 0.008566 | 0.97740 | 0.6123 | 0.995717 | 0.006 | 0.01080 | 2.01778 | 5.76021 | 2.3850 |
| **2** | 0.005587 | 0.968634 | 0.8163 | 0.997207 | 0.013 | 0.018964 | 1.384442 | 3.37708 | 2.98339 |
| **3** | 0.005338 | 0.978297 | 0.7487 | 0.997331 | 0.009 | 0.012767 | 1.655632 | 4.73059 | 2.77234 |
| **4** | 0.005214 | 0.976312 | 0.7746 | 0.997393 | 0.011 | 0.013236 | 1.244131 | 3.33805 | 2.91287 |
| **5** | 0.006642 | 0.973369 | 0.7439 | 0.996679 | 0.011 | 0.019105 | 2.274177 | 7.10785 | 2.68715 |
| **6** | 0.005742 | 0.983522 | 0.6463 | 0.997129 | 0.006 | 0.010301 | 1.605176 | 4.28244 | 2.05357 |
| **7** | 0.008752 | 0.956693 | 0.7892 | 0.995624 | 0.008 | 0.010716 | 1.578003 | 4.13867 | 2.57759 |
| **8** | 0.004593 | 0.969224 | 0.8461 | 0.997703 | 0.010 | 0.01203 | 0.826578 | 2.47775 | 2.77483 |
| **9** | 0.009621 | 0.976871 | 0.5744 | 0.995189 | 0.011 | 0.01429 | 0.945757 | 2.65592 | 2.23901 |
| **10** | 0.00748 | 0.982728 | 0.5598 | 0.99626 | 0.010 | 0.008143 | 0.419944 | 2.28365 | 2.81441 |

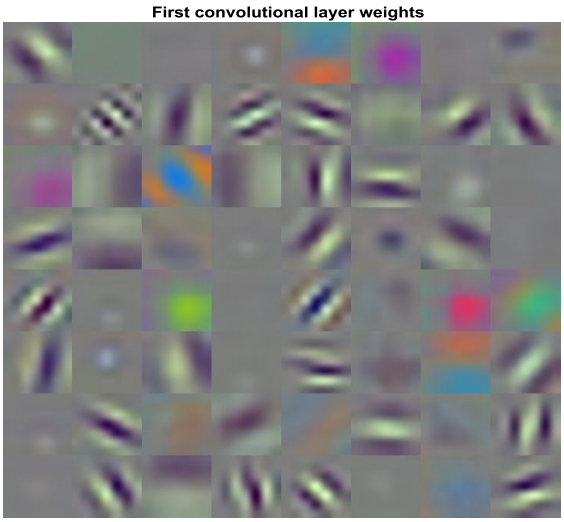

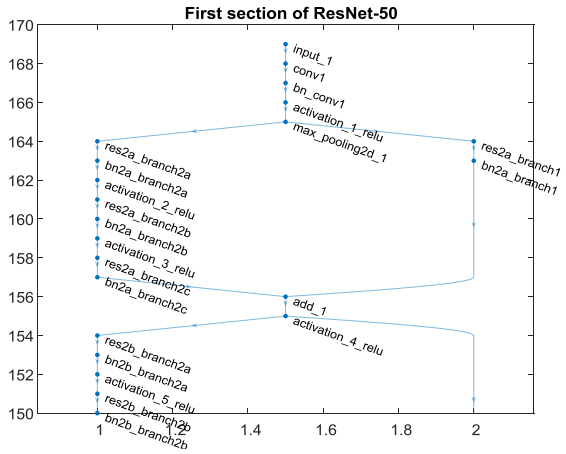


**Figure 7** The First Convolution Layer Weights and First Section of Resnet

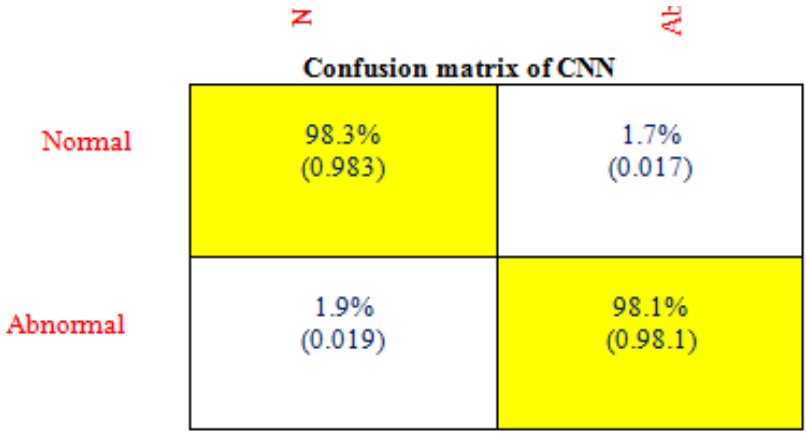


**Figure 8**Confusion Matrix of Proposed CNN

**Table 4**Performance Value of CNN

| classifier | CNN |
|---|---|
| **Accuracy (%)** | 98.3 |
| **Error (%)** | 1.7 |
| **Sensitivity (%)** | 97.9 |
| **Specificity (%)** | 98.62 |
| **Precision (%)** | 96.83 |
| **F1_score** | 0.9521 |

**Table 5**Comparison of Accuracy in different Classifiers

| **Number of test images (normal = 50, abnormal = 50)** | | | | |
|---|---|---|---|---|
| **Evaluation parameter** | **SVM** | **Back Propagation** | ***K*-NN** | **Proposed classifier (CNN)** |
| Specificity (%) | 91.74 | 92.54 | 94.72 | 98.62 |
| Sensitivity (%) | 96.2 | 97.2 | 97.5 | 97.9 |
| Accuracy (%) | 90.03 | 95.46 | 96.51 | 98.3 |

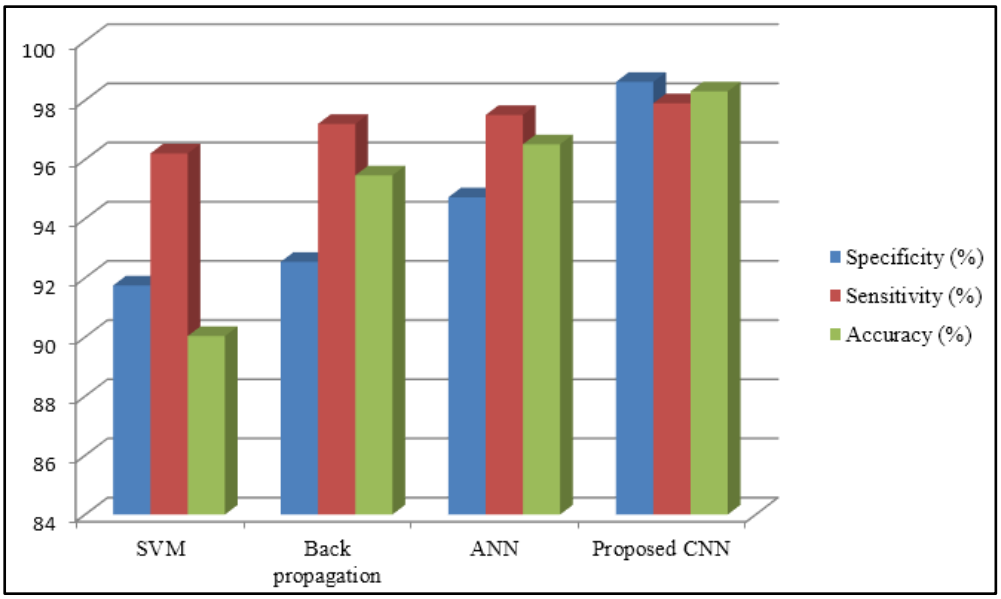


**Figure 9**Comparison Plot of various Classifiers

The ROC Curve shows the contrast of the different classifiers and the classifiers suggested. The True Positive value is high, which means that the approach is higher than some of the other method for easy cancer area analysis.

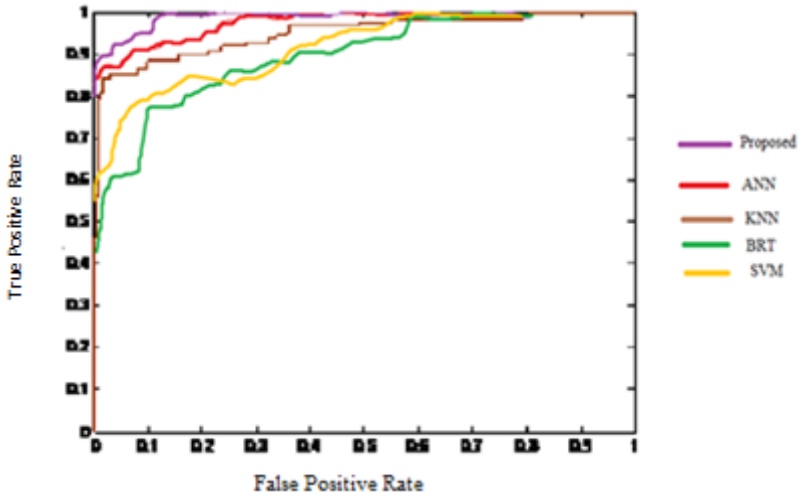


**Figure 10.** ROC Curve for Deep Learning Classifier

The aim of the current paper is to build an effective automated segmentation method for brain tumours by classifying brain tumours as normal and abnormal. A significant contribution to image processing would be made by the use of CNN approaches, which are common and effective methods of segmentation and classification. These techniques can further be used for segmentation and classification of other abnormalities of brain like Parkinson's disease, Alzheimer's disease, stroke, and autism.

## CONCLUSION

In terms of classification, dense convolutional layers neural pathways (CNNs) have been greatly explored in the science and new firms. In this research

paper, evaluate the effectiveness of a deep neural network model for a classification algorithm linked to the diagnosis of brain cancer. The extension applied to the ResNet model shows that the deep learning algorithm used in natural image processing can provide superior efficiency in the analysis of medical data. The proposed device was designed to identify the brain tumour of the Magnetic Resonance Imaging (MRI) brain. There are many phases novel boosted adaptive anisotrophic diffusion filter is used for noise removal, to detect the tumor part from the brain image. Segmentation extracts the tumor portion. Textural feature extraction is used in proposed system. Classification uses CNN classifiers; proposed system achieved 98.3% of accuracy. Future enhancement is to perform with the Perfusion based MRI images which is quite complex.

## REFERENCES

Saba, T., Mohamed, A.S., El-Affendi, M., Amin, J., & Sharif, M. (2020). Brain tumor detection using fusion of hand crafted and deep learning features. *Cognitive Systems Research*, *59*, 221-230.

Sharif, M., Amin, J., Nisar, M.W., Anjum, M.A., Muhammad, N., & Shad, S. A. (2020). A unified patch based method for brain tumor detection using features fusion. *Cognitive Systems Research*, *59*, 273-286.

Toğaçar, M., Ergen, B., &Cömert, Z. (2020). BrainMRNet: Brain tumor detection using magnetic resonance images with a novel convolutional neural network model. *Medical Hypotheses*, *134*, 109531.

Veeramuthu, A., Meenakshi, S., &Darsini, V.P. (2015). Brain image classification using learning machine approach and brain structure analysis. *Procedia Computer Science*, *50*, 388-394. www.sciencedirect.com

Kumar, S., Dabas, C., &Godara, S. (2017). Classification of brain MRI tumor images: A hybrid approach. *Procedia computer science*, *122*, 510-517. www.sciencedirect.com

Jana, G.C., Swetapadma, A., &Pattnaik, P.K. (2018). Enhancing the performance of motor imagery classification to design a robust brain computer interface using feed forward back-propagation neural network.*Ain Shams Engineering Journal*, *9*(4), 2871-2878. www.sciencedirect.com

Sidhu, H.S., Benigno, S., Ganeshan, B., Dikaios, N., Johnston, E.W., Allen, C., & Taylor, S.A. (2017). Textural analysis of multiparametric MRI detects transition zone prostate cancer. *European radiology*, *27*(6), 2348-2358.

Anaraki, A.K., Ayati, M., &Kazemi, F. (2019). Magnetic resonance imaging-based brain tumor grades classification and grading via convolutional neural networks and genetic algorithms. *Biocybernetics and Biomedical Engineering*, *39*(1), 63-74.

Fabelo, H., Ortega, S., Lazcano, R., Madroñal, D., M Callicó, G., Juárez, E., &Piñeiro, J.F. (2018). An intraoperative visualization system using hyperspectral imaging to aid in brain tumor delineation. *Sensors*, *18*(2), 430.

Zhang, J., Shen, X., Zhuo, T., & Zhou, H. (2017). Brain tumor segmentation based on refined fully convolutional neural networks with a hierarchical dice loss. *arXiv preprint arXiv:1712.09093*.

Wang, N., Shang, Y., Chen, Y., Yang, M., Zhang, Q., Liu, Y., &Gui, Z. (2018). A hybrid model for image denoising combining modified isotropic diffusion model and modified Perona-Malik model. *IEEE Access*, *6*, 33568-33582.

Chang, Y., Jung, C., Ke, P., Song, H., & Hwang, J. (2018). Automatic contrast-limited adaptive histogram equalization with dual gamma correction.*IEEE Access*, *6*, 11782-11792.

Haleem, M.S., Han, L., van Hemert, J., Li, B., Fleming, A., Pasquale, L.R., & Song, B.J. (2018). A novel adaptive deformable model for automated optic disc and cup segmentation to aid glaucoma diagnosis. *Journal of medical systems*, *42*(1), 20.

Wang, Y., Karimi, H.R., Shen, H., Fang, Z., & Liu, M. (2018). Fuzzy-model-based sliding mode control of nonlinear descriptor systems. *IEEE transactions on cybernetics*, *49*(9), 3409-3419.

Uziel, R., Ronen, M., &Freifeld, O. (2019). Bayesian Adaptive Superpixel Segmentation. In *Proceedings of the IEEE International Conference on Computer Vision*, 8470-8479.

Pradhan, J., Kumar, S., Pal, A.K., & Banka, H. (2018). A hierarchical CBIR framework using adaptive tetrolet transform and novel histograms from color and shape features. *Digital Signal Processing*, *82*, 258-281.

Yang, F., Dogan, N., Stoyanova, R., & Ford, J.C. (2018). Evaluation of radiomic texture feature error due to MRI acquisition and reconstruction: a simulation study utilizing ground truth. *PhysicaMedica*, *50*, 26-36.

Sihwail, R., Omar, K., Ariffin, K.A.Z., &Tubishat, M. (2020). Improved harrishawks optimization using elite opposition-based learning and novel search mechanism for feature selection. *IEEE Access*, *8*, 121127-121145.

Chuang, T.Y., Han, J.Y., Jhan, D.J., & Yang, M.D. (2020). Geometric Recognition of Moving Objects in Monocular Rotating Imagery Using Faster R-CNN. *Remote Sensing*, *12*(12), 1908.

Ćiprijanović, A., Snyder, G.F., Nord, B., & Peek, J.E. (2020). DeepMerge: Classifying high-redshift merging galaxies with deep neural networks.*Astronomy and Computing*, *32*, 100390.

Sarhan, A.M. (2020). Detection and Classification of Brain Tumor in MRI Images Using Wavelet Transform and Convolutional Neural Network.*Journal of Advances in Medicine and Medical Research*, 15-26.

Singh, S.P., Wang, L., Gupta, S., Goli, H., Padmanabhan, P., &Gulyás, B. (2020). 3D Deep Learning on Medical Images: A Review. *arXiv preprint arXiv:2004.00218*.

Chaubey, N.K., &Jayanthi, P. (2020). Disease Diagnosis and Treatment Using Deep Learning Algorithms for the Healthcare System. In *Applications of Deep Learning and Big IoT on Personalized Healthcare Services,IGI Global*, 99-114.

Joseph, T., Kalaiselvan, S.A., Aswathy, S.U., Radhakrishnan, R., &Shamna, A. R. (2020). A multimodal biometric authentication scheme based on feature fusion for improving security in cloud environment. *Journal of Ambient Intelligence and Humanized Computing*, 1-9.

Aswathy, S.U., Devadhas, G.G., & Kumar, S. S. (2020). A tumour segmentation approach from FLAIR MRI brain images using SVM and genetic algorithm. *International Journal of Biomedical Engineering and Technology*, *33*(4), 386-397.